Journal of Nuclear Materials 438 (2013) S545–S549

Contents lists available at SciVerse ScienceDirect

Journal of Nuclear Materials

journal homepage: www.elsevier.com/locate/jnucmat

Numerical studies of effects associated with the Super-X divertor on target parameters in MAST-U

E. Havlíčková [a,*,1], W. Fundamenski [a], M. Wischmeier [b], G. Fishpool [a], D. Coster [b]

[a] EURATOM/CCFE Fusion Association, Culham Science Centre, Abingdon, United Kingdom
[b] Max-Planck Institut für Plasmaphysik, EURATOM Association, Garching, Germany

ARTICLE INFO

Article history:
Available online 16 January 2013

ABSTRACT

As part of preparations for the new Super-X divertor (SXD) on MAST, the influence of long divertor leg is modelled by SOL transport codes. The SOLPS5.0 package is used to study the effect of the expanded divertor in two dimensions and a comparison between the conventional geometry (standard short divertor) and the SXD geometry is presented. We focus on plasma parameters in the divertor and total particle and energy balance in the SOL. Finally, a one-dimensional SOLF1D code is benchmarked with SOLPS and used to study the effects of longer connection length $L_\parallel$ and magnetic flux expansion $\nabla_\parallel B$ separately.

1. Introduction

Design of the tokamak divertor plays an important role in energy exhaust issues as the divertor geometry influences its performance and closure. One of the concepts with potential for improved performance is the Super-X divertor (SXD) which will be installed at the MAST spherical tokamak [1]. The major role of SXD is to reduce plasma temperatures and heat loads on targets via long connection length and larger target wetted area achieved by magnetic flux expansion (targets at large radius). Additionally, the SXD design gains from improved divertor closure which helps to separate neutrals and impurities from the confined region and the upstream SOL, and which enables to reach higher neutral pressures in the divertor volume.

In this paper, we study the properties of the expanded divertor numerically, using SOL transport codes. First, the SOLPS code [2] is applied to two configurations of MAST-U: (i) the conventional divertor (CD) and (ii) the Super-X divertor, and these cases are compared in conditions of H-mode regime. Beside geometry concepts, SOLPS can also be used to provide scans in other parameters affecting particle and power balance in the SOL, such as the core density (fuelling), the total power input, impurity content or collisionality (L-mode/H-mode regimes with different radial transport properties). These simulations, however, will be presented in detail in a separate paper, as well as validation of SOLPS simulations against MAST experiment, which is underway.

In addition, we compare 2D SOLPS simulations to 1D numerical studies of parallel transport in the SOL carried out by the SOLF1D code [3]. Flexibility of 1D calculations enables to separate effects of the connection length from magnetic flux expansion and run larger scans with varying the length of the divertor, while prescribing any dependence for the magnetic field. The study is initiated by benchmarking of the SOLF1D code with a solution of SOLPS on a flux tube in the SOL. On this flux tube, we model the effects associated with stretching the divertor region, while assuming static sources due to cross-field transport in the upstream SOL and recycling sources in the divertor volume based on the EIRENE calculation. The effects of $L_\parallel$ and $\nabla_\parallel B$ are measured by investigating target quantities such as plasma temperatures or energy fluxes.

2. Effect of the Super-X divertor in 2D

Simulations of SOLPS for the conventional and SXD geometry (defined in Fig. 1) represent the baseline of the presented work. Results are shown as a comparison between short and long leg designs focusing on the divertor performance, while keeping the same upstream SOL conditions. The reference case is connected double null with deuterium plasma in H-mode. No impurity is present. The total power to the grid is $P_{inp} = 1.7$ MW and the core density is $n_{core} = 2.8 \times 10^{19}$ m^{-3} (density at the innermost ring of the SOLPS grid located 5 cm inside separatrix at the outer midplane). Transport coefficients are $D_\perp = \chi_\perp = 1$ m^2 s^{-1} in the SOL, $D_\perp = \chi_\perp = 2$ m^2 s^{-1} in the core and reduced to $D_\perp = 0.2$ m^2 s^{-1} and $\chi_\perp = 0.5$ m^2 s^{-1} in the region extending 2 cm inside and 0.5 cm outside the separatrix. A similar case has been preliminarily studied in [4].

While the midplane temperatures and densities are almost identical in both configurations ($T_{e,sep} \approx 100$ eV, $n_{e,sep} \approx 9 \times 10^{18}$ m^{-3}) and there is only a small change in plasma quantities in the divertor on the inner side, we observe a steep reduction of temperatures and increase of plasma density at the outer targets of SXD. The radial

* Corresponding author. Address: Culham Centre for Fusion Energy, Culham Science Centre, Abingdon OX14 3DB, United Kingdom.
E-mail address: eva.havlickova@ccfe.ac.uk (E. Havlíčková).
[1] Presenting author.

0022-3115/$ - see front matter © 2013 Elsevier B.V. All rights reserved.
http://dx.doi.org/10.1016/j.jnucmat.2013.01.113

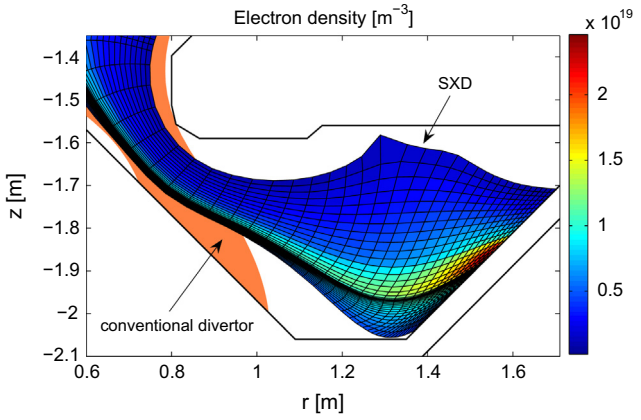

Fig. 1. SXD versus conventional divertor of MAST-U and electron density n_e calculated by SOLPS. In SXD, additional poloidal field coils in the divertor are employed pulling the divertor leg to larger radius and reducing the poloidal magnetic field in the divertor volume, see [4]. The latter leads to the expansion of flux tubes and increased connection length in the divertor.

Table 1
Power and particle balance in CD and SXD. P_{core} is the power lost in the core, $P_{sol,in}$ or $P_{sol,out}$ is the power crossing the core/SOL boundary on the inner or outer side, $P_{t,out}$ or $P_{t,in}$ is the power deposited at the outer or inner targets, P_{wall} is the power deposited at both inner and outer walls, P_{pfr} is the power crossing the boundary in private flux regions, P_{vol} is the power lost in the SOL. The above quantities are calculated with respect to the total power input P_{inp} = 1.7 MW. Notation is analogous for the particle flux Γ. $\Gamma_{sol,out}$ is with respect to Γ_{sol} and $\Gamma_{wall,out}$ with respect to $\Gamma_{t,out}$.

	CD	SXD
P_{core}	4%	4%
$P_{sol,in}$, $P_{sol,out}$	12%, 84%	10%, 86%
$P_{t,in}$, $P_{t,out}$	14%, 78%	13%, 59%
P_{wall}, P_{pfr}	1%, 0%	2%, 4%
P_{vol}	3%	18%
Γ_{sol}	4.4×10^{21} s^{-1}	4×10^{21} s^{-1}
$\Gamma_{sol,out}$	81%	81%
$\Gamma_{t,out}$	2×10^{21} s^{-1}	6×10^{21} s^{-1}
$\Gamma_{wall,out}$	3%	2%

decay length for n_e at the outboard midplane (index u as *upstream*) is approximately $\lambda_n^u \approx 7$ mm ($\lambda_n = n_e/|\nabla n_e|$) in the near SOL (transport barrier) and 20–30 mm in the far SOL and for T_e ranges from 3 to 20 mm.

The effect of SXD on target power loads is shown in Fig. 2. The peak power load Q_t is reduced by a factor of 4.5 and the effective flux expansion accounts for a factor of 4.27 of the drop. At the top of Fig. 2, we can see the energy and particle fluxes perpendicular to the plate, at the bottom, parallel energy and particle fluxes are shown, all as functions of the plate coordinate y. While the peak particle load remains unchanged, Fig. 2b, the peak power load is reduced, Fig. 2a. Two effects are responsible for this reduction – magnetic flux expansion (toroidal and poloidal) and target plate tilting. The target tilting can be excluded by comparison of the poloidal energy flux (related to the target flux as $Q_t = Q_{pol}\sin\beta$ where β is the tilting angle), which is reduced by factor of 3.4. The energy flux parallel to the magnetic field (related to the poloidal flux as $Q_{pol} = Q_\parallel B_\theta^t/B^t$ where B_θ^t/B^t corresponds to the local pitch angle) drops by factor of 1.6, Fig. 2c. Decay lengths at the target λ_Q^t and λ_Γ^t (index t as *target*) indicate broadening of target loads radially, although λ_Q mapped to the midplane is comparable in both cases, $\lambda_Q^u \approx \lambda_Q^t/\langle dy/dr\rangle \approx 3$ mm. The effective flux expansion $FX_{eff} \equiv \langle FX\rangle$ defined as the average of $FX \equiv R^t dy/R^u dr$ over λ_Q^t is approximately $FX_{eff} \approx \langle FX_\theta\rangle \times \langle FX_\varphi\rangle \times \langle FX_{tilt}\rangle$ which is $6.02 \approx 3.4 \times 0.61 \times 2.89$ for the CD case and $25.73 \approx 6.73 \times 1.17 \times 3.24$ for the SXD case. The magnetic flux expansion is defined as $FX_\theta \equiv B_\theta^u B^t/B^u B_\theta^t$ (poloidal) and $FX_\varphi \equiv R^t/R^u$ (toroidal) and flux expansion due to the target tilting is defined as $FX_{tilt} \equiv 1/\sin\beta$. The effective flux expansion gives a reduction of the total energy flux in SXD by factor of 4.27 with respect to CD, with $\langle FX_\theta\rangle$ factor of 1.98 larger, $\langle FX_\varphi\rangle$ factor of 1.92 larger and expansion due to target tilting $\langle FX_{tilt}\rangle$ 1.12 times larger.

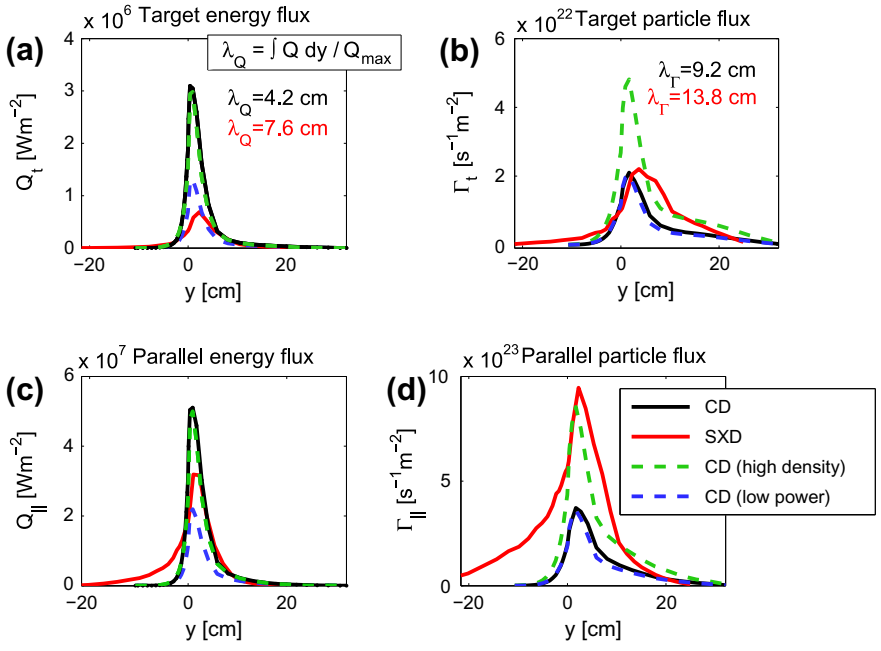

Fig. 2. Energy and particle fluxes deposited at the outer target as calculated by SOLPS. Comparison of CD (black) and SXD (red). Two additional cases for CD, one with increased fuelling $n_{core} = 5 \times 10^{19}$ m^{-3} and the second one with reduced power P_{inp} = 0.84 MW, are shown in green and blue. The coordinate y coincides with the target plate in the poloidal plane (r, z) and ranges from −20 cm in the private flux region up to 30 cm in the far SOL, with 0 corresponding to the strike point location. (For interpretation of the references to color in this figure legend, the reader is referred to the web version of this article.)

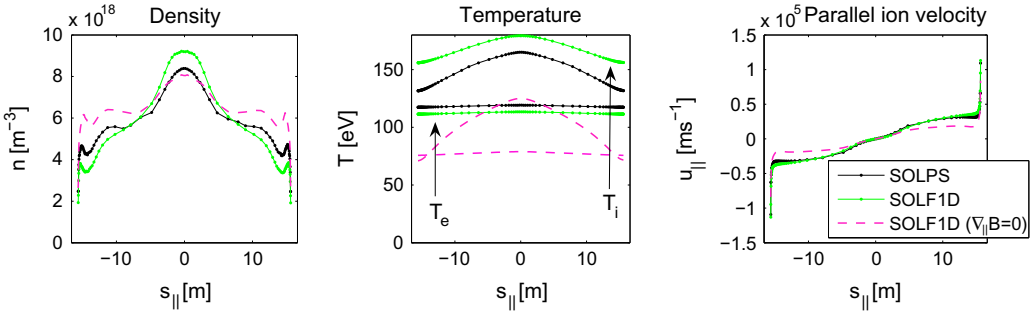

Fig. 3. Solution of SOLF1D (green) along a flux tube compared versus SOLPS solution (black) for the CD case. The third solution (magenta) is a results of SOLF1D for $\nabla_{\|}B = 0$ along the flux tube. (For interpretation of the references to color in this figure legend, the reader is referred to the web version of this article.)

It should be mentioned that the field line angle at the target is reduced in the SXD scenario due to low poloidal magnetic field in the divertor and the SXD equilibrium studied here allows very small field line angles around the critical value of 1°.

Two additional cases have been performed for the short divertor in an attempt to reduce target power loads by the main control parameters – n_{core} and P_{inp}, and to compare the effect with the impact of geometry. The SXD configuration results in factor of 2 stronger reduction of target power loads at $P_{inp} = 1.7$ MW than the standard divertor with 2 times smaller P_{inp}, Fig. 2a. Moreover, increased fuelling does not affect the maximum power load, but leads to higher particle flux Γ_t at the target, Fig. 2b and d, and reduced temperatures.

Power and particle balance is summarized in Table 1. Most of the power and particles cross the core/SOL boundary on the outer side for poloidally uniform radial transport coefficients. In both configurations, the power is mainly deposited on the outer targets, while only a small fraction arrives at the walls (this fraction would be larger in L-mode with stronger radial transport). The volumetric power loss in the SOL is increased in SXD, favouring the long leg geometry.

3. Comparison of SOLPS and SOLF1D

For the purpose of application of the SOLF1D model to MAST, the model is benchmarked with parallel transport in SOLPS. The SOLF1D model follows generalized equations taking into account the effect of $\nabla_{\|}B$ as documented, e.g. in [5] and the parallel variation of the magnetic field on a given flux tube is prescribed as in SOLPS. The recycling sources in the divertor are taken from EIRENE and sources due to flows across the flux tube are calculated from SOLPS fluxes. Figs. 3 and 4 show a comparison between the two codes for two studied geometries from Fig. 1. The comparison of solutions is presented for $n_e = n_i$, T_e, T_i and $u_{\|,i}$ on a flux tube in the outer SOL close to the separatrix, where the maximum target power load in SOLPS is observed. While for the SXD case (high-recycling SOL with steep temperature gradients), the agreement is nearly perfect (Fig. 4), for the CD case (sheath-limited SOL), discrepancies up to 15% are evident (Fig. 3). These discrepancies are caused to some extent by differences between the models (boundary conditions for T_i differ and it has been proven that T_i match well if the same boundary conditions are used). Additional discrepancies (in n_e and T_e) are likely caused by inaccuracy due to discretization. A detailed benchmark of the codes will be published separately. In addition, Figs. 3 and 4 show the effect of the $\nabla_{\|}B$ force, investigated also in [6].

The target fluxes resulting from SOLF1D for the case from Fig. 3 are $Q_{\|,e} = 19.5$ MW m^{-2}, $Q_{\|,i} = 19.1$ MW m^{-2} and $\Gamma_{\|} = 2.2 \times 10^{23}$ m^{-2} s^{-1}. The solution of SOLF1D in Fig. 3 plotted as dashed line is obtained with constant magnetic field along the whole flux tube, indicating that $\nabla_{\|}B$ option in SOLF1D is important for MAST (less so for conventional aspect ratio tokamaks). Sources and parallel transport in SXD (Fig. 4) are more dominated by recycling. For the same upstream density, the target density is larger due to ionization sources. Temperatures in the divertor are reduced due to cooling by plasma-neutral interaction and additional energy flux expansion in SXD (the divertor placed at larger radius). The target fluxes are $Q_{\|,e} = 16.8$ MW m^{-2}, $Q_{\|,i} = 8.3$ MW m^{-2} and $\Gamma_{\|} = 8.3 \times 10^{23}$ m^{-2} s^{-1}. The solution plotted as dashed line in Fig. 4 shows the effect of $\nabla_{\|}B$ in the divertor region, by taking into account the same poloidal variations of B in the SOL, but keeping B constant in the divertor (effectively expanding the divertor vertically instead of radially, see the following section). The target fluxes in this case increase as $Q_{\|,e} = 35.6$ MW m^{-2}, $Q_{\|,i} = 18.8$ MW m^{-2} and $\Gamma_{\|} = 8.7 \times 10^{23}$ m^{-2} s^{-1}.

4. 1D stretching of the divertor leg

Starting with the reference CD case in Fig. 3, a 1D analysis is carried out based on stretching a flux tube in the outer SOL (Fig. 5 left) in two directions labelled as (a) and (b). The magnetic field along the flux tube corresponding to these two directions is plotted in Fig. 5 on the right[2] (blue) and compared to the original CD case from Fig. 3 (black) and the SXD case from Fig. 4 (red). The treatment of sources during stretching is not well defined and the sources cannot be modelled self-consistently in 1D (the recyling sources change with the flux to the divertor which is affected by increasing $L_{\|}$ or changing B, plus 2D processes are involved). We treat the radial and recycling sources ($S = S_{\perp} + S_{rec}$) separately and assume that $S_{\perp}$, which is largest in the upstream SOL and around X points, does not change during stretching. For the recycling source, we employ two methods: (1) We assume that the total integrated recycling source/sink $\int S_{rec}$ in the divertor is constant while expanding the flux tube. This approach shows the effect of magnetic flux expansion exclusively. (2) We assume that the integrated recycling source $\int S_{rec}$ grows linearly with the length of the divertor leg. This approach adds the effect of plasma-neutral interaction and partially incorporates 2D effects as we would expect the source due to recycling to be stronger with larger divertor volume. The second method is supported by results of SOLPS simulations, which show for SXD approximately 4 times larger source due to ionization, factor of 4 stronger electron cooling in the divertor, but comparable cross-field transport sources. While the particle source is dominated by ionization of recycled neutrals, the energy source is dominated by cross-field transport. That is why the total energy source term $\int S^E/B ds_{\|}$ (determining the energy flux at the target as $\int S^E/B ds_{\|} = Q_{\|}/B_t$) is effectively the same for SXD as for the short divertor for approximately twice as long connection length. The target energy flux is

[2] For interpretation of color in Fig. 5, the reader is referred to the web version of this article.

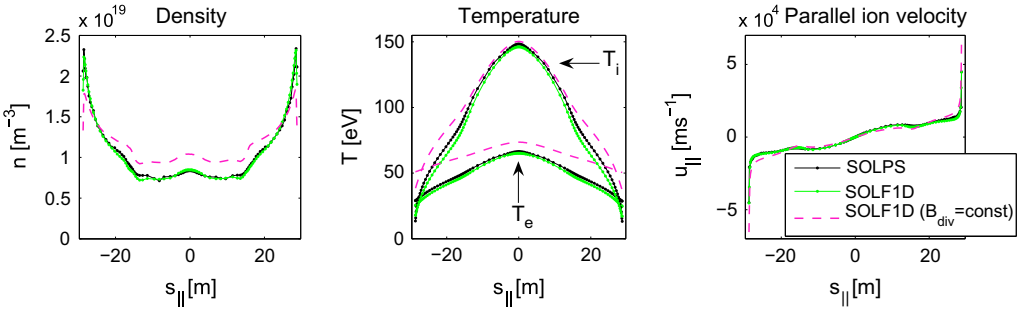

Fig. 4. The same as in Fig. 3, but for the SXD case. The solution in dashed line (magenta) is a result with constant magnetic field in the divertor B_{div} = const.

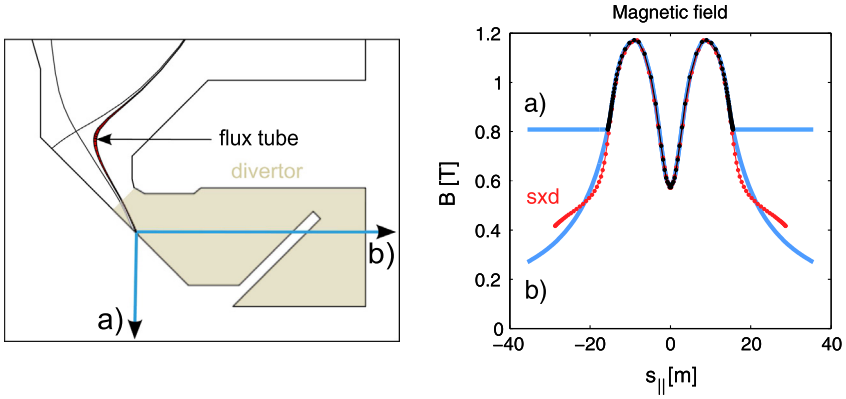

Fig. 5. The scheme on the left shows a flux tube from SOLPS and different ways of stretching the divertor in 1D: (a) vertical stretching (constant magnetic field), (b) radial stretching (decreasing magnetic field as $B \propto 1/R$). The graph on the right shows the magnetic field considered in the 1D code.

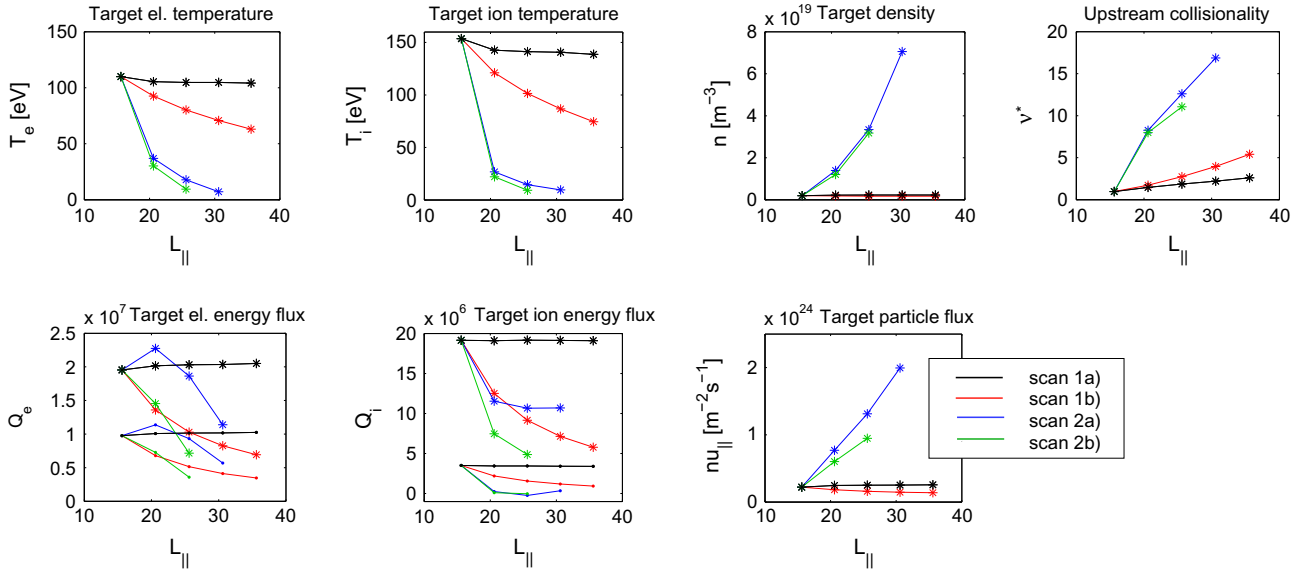

Fig. 6. Parameters at the target calculated by SOLF1D as functions of the connection length, based on four scans involving stretching of the divertor region as described in the text. The bottom branches in Q_e and Q_i are conductive components of the energy flux.

then approximately 1.6 times smaller as a result of smaller magnetic field at the target $B_t \approx 0.4$ T, compared to $B_t \approx 0.8$ T in the short divertor.

Different treatment of sources in the flux tube (1) versus (2) described above and different directions of stretching the flux tube (a) versus (b) from Fig. 5 give a combination of 4 scans, each shown in different color in Fig. 6: (1a) In case of vertical stretching (no additional flux expansion), the target quantities do not change and both the particle and energy fluxes remain the same with increasing $L_{\parallel}$. This is not surprising as $\int S^E/B ds_{\parallel}$ and $\int S^n/B ds_{\parallel}$ do not change with constant magnetic field in the divertor. (1b) Radial stretching (the magnetic field drops in the divertor as $B \propto 1/R$) leads already to a large reduction of temperatures and energy fluxes. (2a) With more recycling in the divertor, i.e. larger particle source and more cooling (the recycling sources scale with the divertor volume), the temperature drop is much steeper even with-

out magnetic flux expansion (vertical stretching), however, with less effect on the energy fluxes than flux expansion alone in the previous case. (2b) The most beneficial is the combination of both effects, which results in a substantial drop of both temperature and energy fluxes, increased density and particle flux, and higher collisionality.

5. Conclusions

2D simulations of MAST-U Super-X divertor (targets at 2 times larger radius, twice longer $L_{\|}$) show a significant reduction of plasma target temperatures temperatures ($T_{e,t}$ drops from 126 eV to 38 eV, $T_{i,t}$ from 132 eV to 13 eV) and maximum power loads (from 3.1 MW m^{-2} to 0.7 MW m^{-2}) at the outer targets compared to the conventional divertor with the same conditions in the core and upstream SOL, and comparable plasma parameters on the inner side of the tokamak. The reduction of power loads occurs mainly due to magnetic flux expansion and partially due to target tilting, both increasing the target wetted area. Plasma and neutral densities in the outer divertor are larger ($n_{e,t}$ rises from 0.5 to 2.2×10^{19} m^{-3}), while the maximum particle load to the targets remains the same. It is worth noting, that in both divertor geometries, additional fuelling does not reduce the target power loads under attached divertor conditions, although it clearly does increase the particle load and recycling.

Finally, 1D parallel transport model was used to estimate the effects of stretching the divertor region in two directions – vertically and radially, and the influence of $L_{\|}$ and $\nabla_{\|}B$ on parallel target fluxes, temperatures and density was quantified. It was found that magnetic flux expansion in the divertor has a strong impact on the target energy fluxes, but has less influence on the density and temperatures in the divertor in comparison to enhanced recycling (larger recycling plasma source and electron cooling in the expanding divertor).

Acknowledgements

This work was supported by EURATOM and carried out within the framework of the European Fusion Development Agreement. The views and opinions expressed herein do not necessarily reflect those of the European Commission. The CCFE authors were funded by the RCUK Energy Programme under Grant No. EP/I501045.

References

[1] P.M. Valanju, Phys. Plasmas 16 (2009) 056110.
[2] R. Schneider et al., Contrib. Plasma Phys. 46 (2006) 3.
[3] E. Havlíčková et al., Plasma Phys. Control. Fusion 53 (2011) 065004.
[4] S. Lisgo et al., ECA 33E (2009). O-4.046.
[5] E. Zawaideh et al., Phys. Fluids 29 (1986) 463.
[6] A. Kirk et al., Plasma Phys. Control. Fusion 45 (2003) 1445.